Superconductivity in the complex metallic alloy β-Al_3Mg_2

E. Bauer, H. Kaldarar, R. Lackner, H. Michor, and W. Steiner
Institut für Festkörperphysik, Technische Universität Wien, A-1040 Wien, Austria

E.-W. Scheidt
Lehrstuhl für Chemische Physik und Materialwissenschaften, Universität Augsburg, D-86159 Augsburg, Germany

A. Galatanu
National Institute for Materials Physics, 77125 Magurele, Romania

F. Marabelli
Physics Department "A. Volta," University of Pavia, I-27100 Pavia, Italy

T. Wazumi and K. Kumagai
Division of Physics, Graduate School of Science, Hokkaido University, Sapporo 060-0810, Japan

M. Feuerbacher
Forschungszentrum Jülich GmbH, D-52425 Jülich, Germany

(Received 19 March 2007; revised manuscript received 6 June 2007; published 26 July 2007)

Transport and thermodynamic properties were studied for the complex metallic compound β-Al_3Mg_2, composed of 925 atoms per unit cell. β-Al_3Mg_2 exhibits bulk superconductivity below $T_c=0.87$ K. An exponential temperature dependence of the specific heat well below T_c indicates BCS-like behavior with a nodeless gap of width $\Delta_{BCS}(0)\approx 1.5$ K. The coherence length is derived as $\xi_0=4.85\times 10^{-8}$ m and the Ginzburg Landau parameter $\kappa_{GL}\approx 13$, characterizing β-Al_3Mg_2 as a type II superconductor. Superconductivity in β-Al_3Mg_2 occurs in the absence of inversion symmetry of the crystal. Surprisingly, in spite of the rather complex crystal structure of β-Al_3Mg_2, physical properties turn out to be quite simple.

DOI: 10.1103/PhysRevB.76.014528 PACS number(s): 74.25.Bt, 74.70.Ad, 72.15.Eb

I. INTRODUCTION

Structurally complex metallic alloy phases (CMAs) are remarkable metallic systems based on crystal structures composed of several hundreds or even thousands of atoms per unit cell. Although known for a long time, a systematic study of physical properties was commenced only recently because of the availability of high quality sample material, in some cases, also of single crystals.

The earliest investigated compound in this family is $NaCd_2$ with 1125 atoms per unit cell.[1] Others are the Bergman phases $Mg_{32}(Al,Zn)_{49}$ with 162 atoms per unit cell[2] or ξ'-$Al_{74}Pd_{22}Mn_4$ with 320 atoms per unit cell.[3] Today, a significant number of intermetallic compounds are known, having complex structures with huge number of atoms per unit cell. For a recent review, see, e.g., Ref. 4.

Complex metallic alloys are characterized by the occurrence of different length scales, with a lattice periodicity of several nanometers, but clusterlike atomic arrangements on a nanometer scale. Hence, CMAs are periodic crystals but on an atomic scale resemble quasicrystals. Such competing scales are supposed to trigger emergent physical properties inherent in these specific materials.

The present investigation is devoted to β-Al_3Mg_2, which, for the first time, was studied in detail with respect to its crystallography by Samson.[5] β-Al_3Mg_2 was classified as a cubic system with space group $Fd\bar{3}m$ and lattice parameter $a=2.8$ nm. 1168 atoms compose the unit cell. The coordination polyhedra consist of icosahedra, Friauf polyhedra, and other polyhedra with various ligancies; for details, see, e.g., Ref. 4. Of particular interest is intrinsic disorder due to mismatching of the various adjacent polyhedra. This cause displacement and substitutional disorder, as well as fractional site occupation.

The possibility of synthesizing high quality single crystals led to a reinvestigation of the Al-Mg phase diagram.[6] The β phase with the composition $Al_{61.5}Mg_{38.5}$ was found to undergo a structural phase transition at $T=214$ °C from the high temperature cubic phase to a trigonal phase with space group $R3m$. In a hexagonal representation, the lattice parameters deduced are $a=1.996$ nm and $c=4.891$ nm, assembling a total of 925 atoms per unit cell.[6] A particular feature of this crystal structure is the absence of inversion symmetry.

The regular arrangement of various species of atoms in such huge unit cells may form a very complex structured electronic density of states (DOS), particularly around the Fermi energy E_F. Additionally, these atoms, coupled together in the solid, are expected to create numerous distinctly different phonon modes, with the resulting phonon spectrum being substantially different from the simple Debye spectrum. Coupling of the conduction electrons with the lattice vibrations of the crystal is a possible cause of superconductivity. In fact, our low temperature study devoted to β-Al_3Mg_2 evidenced bulk superconductivity at $T_c=0.87$ K. Thus, the aim of the present paper is to characterize superconductivity of this material and to derive relevant physical parameters in both the normal and the superconducting state. Various normal state properties regarding β-Al_3Mg_2 were recently investigated by Dolinsek *et al.*[7]

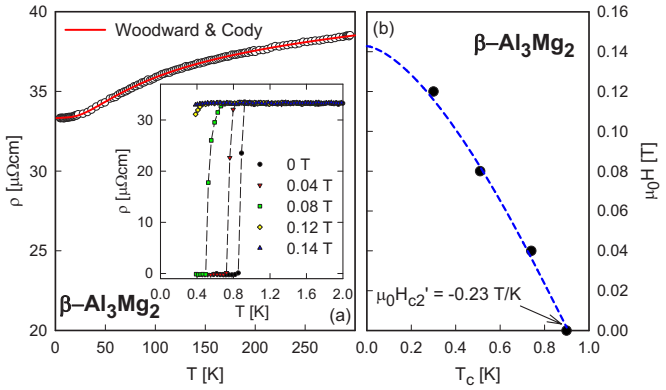

FIG. 1. (Color online) (a) Temperature dependent electrical resistivity ρ of β-Al_3Mg_2. The solid line is a least squares fit according to Eq. (1). The inset shows the onset of a superconducting transition at $T_c^{mid}=0.9$ K. The application of magnetic fields suppresses superconductivity. (b) Temperature dependent upper critical field H_{c2}. The dashed line corresponds to $H_{c2}(T)$ derived in terms of the model of Werthamer *et al.* (Ref. 12) for $\alpha=\lambda_{so}=0$, revealing $\mu_0 H'_{c2} \approx -0.23$ T/K.

II. EXPERIMENT

The samples investigated here belong to the same batch of material as described in Ref. 6. Pieces of β-Al_3Mg_2 were cut from a single crystal grown according to the flux-growth technique.[8] After the growth process, the samples were subjected to a heat treatment at 190° C for 48 h, ensuring that they are in the low temperature trigonal phase. All investigations described in this study were carried out below room temperature.

Bulk properties of β-Al_3Mg_2 were studied in the temperature range from 100 mK up to room temperature. Field and temperature dependent resistivity was measured in a ^{3}He cryostat (400 mK up to 100 K) in fields up to 12 T and in a standard He cryostat from 4.2 K to room temperature. Heat capacity studies were performed at temperatures ranging from 1.5 K up to 120 K by means of a quasiadiabatic step heating technique. Specific heat data were also collected at temperatures down to about 100 mK in a ^{3}He/^{4}He cryostat using a relaxation method.[9] Optical reflectivity at room temperature has been measured over the spectral range from 16 meV up to 6 eV. Spectroscopic ellipsometry has been used from 1.4 to 5 eV. ^{27}Al-NMR was performed with a pulse Fourier transform spectrometer in a superconducting magnet of 9.4 T between 300 and 4.3 K.

III. RESULTS AND DISCUSSION

A. Bulk properties

The temperature dependent electrical resistivity $\rho(T)$ of β-Al_3Mg_2 is shown in Fig. 1(a). As an overall feature, $\rho(T)$ of β-Al_3Mg_2 exhibits a residual resistivity ratio of about 1.16 only, with a residual resistivity $\rho_0 \approx 33$ $\mu\Omega$ cm. The latter can be considered as evidence of significant intrinsic disorder, originated by distinct features of the crystal structure and/or reduced carrier density. In agreement with previous results of Dolinsek *et al.*,[7] the resistivity at low temperatures follows roughly a power law with $\rho=\rho_0+AT^2$, implying electron-electron interaction in metals. At more elevated temperatures, however, the resistivity of β-Al_3Mg_2 is characterized by a strong curvature, which cannot be accounted for in terms of standard models for metallic compounds. Particularly, the Bloch-Grüneisen law fails to describe the interaction of electrons with thermally excited phonons in β-Al_3Mg_2. Rather, the overall $\rho(T)$ dependence of β-Al_3Mg_2 follows the model of Woodward and Cody,[10] which initially was applied to A15 superconductors such as Nb_3Sn. This model reads

$$\rho = \rho_0 + \rho_1 T + \rho_2 \exp(-T_0/T), \tag{1}$$

where ρ_0 is the residual resistivity; ρ_1, ρ_2, and T_0 are material dependent parameters. The second and third terms of Eq. (1) represent the high and low temperature limits of the occupation number of a particular phonon, which assists in interband scattering according to Wilson's model.[11] A more detailed discussion on the temperature dependent resistivity of various superconductors in the normal state region is also given in Ref. 11. A least squares fit of Eq. (1) to the experimental data of β-Al_3Mg_2 is shown in Fig. 1 as a solid line, revealing excellent agreement between the model and data for $\rho_0=33.3$ $\mu\Omega$ cm, $\rho_1=0.0035$ $\mu\Omega$ cm/K, $\rho_2=5.64$ $\mu\Omega$ cm, and $T_0=95$ K.

Measurements performed below 4 K [inset, Fig. 1(a)] demonstrate that β-Al_3Mg_2 undergoes a sharp superconducting transition around 0.9 K. The application of a magnetic field lowers the transition temperature which finally becomes suppressed at the upper critical field $\mu_0 H_{c2}(0) \approx 0.14$ T. These data allow to establish the temperature dependence of $\mu_0 H_{c2}$, displayed in Fig. 1(b). In comparison, superconductivity of pure fcc Al is characterized by $T_c=1.14$ K and a critical field $\mu_0 H_c(0)=0.0105$ T (type I superconductor). Superconductivity was not yet found for Mg.

Werthamer *et al.*[12] derived an expression for the upper critical field $H_{c2}(0)$ in terms of orbital pair breaking, including the effect of Pauli spin paramagnetism and spin-orbit scattering. For dirty limit superconductors, $H_{c2}(0)$ follows from

$$H_{c2}(0) = 0.69 |H'_{c2}| T_c. \tag{2}$$

Equation (2) corresponds to $\alpha=0$ and $\lambda_{so}=0$, where α is the Maki parameter and λ_{so} the spin-orbit scattering parameter. The latter has been shown to increase with increasing atomic numbers of the composing elements[13] and is thus expected to be small for β-Al_3Mg_2. The Maki parameter α can be estimated via the Sommerfeld value of the specific heat γ and the residual resistivity ρ_0,[12]

$$\alpha = \frac{3e^2\hbar\gamma\rho_0}{2m\pi^2 k_B^2}, \tag{3}$$

with e the electron charge and m the electron mass. Taking the experimental residual resistivity and the Sommerfeld value (see below) yields $\alpha=0.11$. Note that a similar value can be derived from[14]

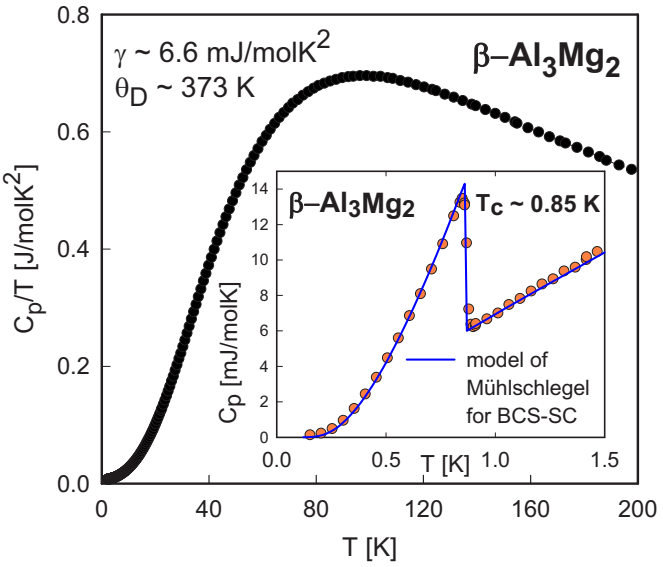

FIG. 2. (Color online) Temperature dependent specific heat C_p of β-Al_3Mg_2 plotted as C_p/T vs T. The inset shows low temperature heat capacity data, evidencing bulk superconductivity. The solid line adjusts the numerical data of Mühlschlegel (Ref. 17) to the present experiment.

$$\alpha = 5.3 \times 10^{-5} \left[\frac{-dH_{c2}(T)}{dT} \right] \Bigg|_{T=T_c} \approx 0.12, \qquad (4)$$

for an initial slope of the upper critical field $\mu_0 H'_{c2} = -0.23$ T/K [compare Fig. 1(a)]. Regarding the concerned lightweight elements Al and Mg, as well as $\alpha \approx 0.1$, we used $\alpha = 0$ and $\lambda_{so} = 0$ for a description of $H_{c2}(T)$ of β-Al_3Mg_2. Results are shown as dashed line in Fig. 1(b), revealing $\mu_0 H_{c2}(0) \approx 0.143$ T and a reasonable agreement with the experimental data.

Orbital pair breaking is the most relevant mechanism in the low field limit and therefore determines H'_{c2}. The Maki parameter $\alpha \approx 0.1$ of β-Al_3Mg_2 corresponds with a dominating orbital field, while for $\alpha \to \infty$, orbital limiting can be neglected. Then, Pauli limiting would allow for an upper critical field of more than 1 T.

Measurements of the temperature dependent specific heat C_p of β-Al_3Mg_2 evidence superconductivity as bulk effect, not originated from spurious phases. Results are shown in Fig. 2.

The heat capacity C_p of β-Al_3Mg_2 is plotted in the main panel of Fig. 2 as C_p/T vs T for temperatures $T > T_c$. Applying the standard analysis to the low temperature data yields a Sommerfeld coefficient $\gamma = 6.6$ mJ/mol K^2 and a Debye temperature $\theta_D = 373$ K. The Debye temperatures of the lightweight elements Al and Mg are 394 and 318 K, respectively. A weighted average of these temperatures roughly coincides with θ_D of β-Al_3Mg_2. Debye temperatures of similar magnitude were previously reported for related icosahedral cluster substructures based on Al.[15] The Sommerfeld values of Al and Mg are 1.35 and 1.3 mJ/mol K^2, respectively, yielding an average of 1.33 mJ/g at K^2. In comparison, β-Al_3Mg_2 results in 1.21 mJ/g at K^2. However, it should be noted that the above outlined analysis for $T > T_c$ holds only for a very narrow temperature range, indicating that the simple Debye model is insufficient to adequately describe the phonon dynamics of this system. A more elaborate model takes into account a more realistic phonon density of states (see below).

Within the McMillan model, both quantities together, i.e., γ and θ_D, determine the superconducting transition temperature T_c:[16]

$$T_c = \frac{\theta_D}{1.45} \exp\left[\frac{-1.04(1+\lambda)}{\lambda - \mu_c^*(1+0.62\lambda)} \right], \qquad (5)$$

with λ as a dimensionless electron-phonon coupling constant, related in terms of the Eliashberg theory to the phonon density of states. λ determines the attractive part of the Cooper pair bonding, while μ^* is the repulsive screened Coulomb part, frequently set to ≈ 0.13. Applying this simple model yields $\lambda = 0.42$, indicating a weakly coupled superconductor.

The inset of Fig. 2 summarizes the heat capacity measurement below 1.5 K. Clearly observable is the specific heat anomaly below 1 K, which, in agreement to the resistivity data, is considered as a signature of bulk superconductivity. Idealization of the heat capacity anomaly under the constraint of entropy balance between the superconducting and the normal state yields $T_c = 0.87$ K. The jump of the specific heat $\Delta C_p/T(T=T_c) \approx 8.5$ mJ/mol K^2 allows calculation of the parameter $\Delta C_p/(\gamma_n T_c) \approx 1.41$, which matches closely the figure expected from BCS theory $[\Delta C_p/(\gamma T_c) \approx 1.43]$. BCS-type superconductivity follows also from an application of the data set of Mühlschlegel[17] to the heat capacity results of β-Al_3Mg_2. Results of this procedure are shown as a solid line in the inset of Fig. 2, revealing fine agreement with the fully gapped BCS superconductivity. Applying the BCS formula for the electronic contribution to the specific heat well below T_c, i.e.,

$$C_{es} = 8.5 \gamma T_c \exp\left[-0.82 \frac{\Delta_{BCS}(0)}{k_B T} \right], \qquad (6)$$

reveals a gap width $\Delta_{BCS}(0)$ of the order of 1.5 K, as well as $\gamma = 6.5$ mJ/mol K^2, in excellent agreement with the Sommerfeld value deduced from the normal state region. This gap width is also consistent with $\Delta = 1.76 T_c = 1.58$ K, if Δ is expressed in kelvin. The thermodynamic critical field is calculated from the free energy difference between the superconducting and normal states: $\Delta F(T) = F_n - F_s = \mu_0 H_c^2(T)/2 = \int_{T_c}^{T} \int_{T_c}^{T'} \frac{(C_s - C_n)}{T''} dT'' dT'$. $C_s(T)$ is obtained from the zero field specific heat measurement and $C_n(T)$ is taken from an extrapolation of the normal state specific heat by $C_n(T) = \gamma T + \beta T^3$. The value $\mu_0 H_c(0) \approx 7.6(2)$ mT obtained for β-Al_3Mg_2 is slightly reduced as compared to Al with $\mu_0 H_c(0) \approx 10.5$ mT, approximately by the same factor as T_c.

In order to obtain more aspects on the lattice dynamics of β-Al_3Mg_2, we employ in Fig. 3 a $(C_p - \gamma T)/T^3$ vs $\ln T$ representation. This particular representation allows us to emphasize deviations from the simple Debye model, which, at low temperatures, follows $Cp \propto T^3$. Note that the Sommerfeld value extrapolated from the normal state region, γ

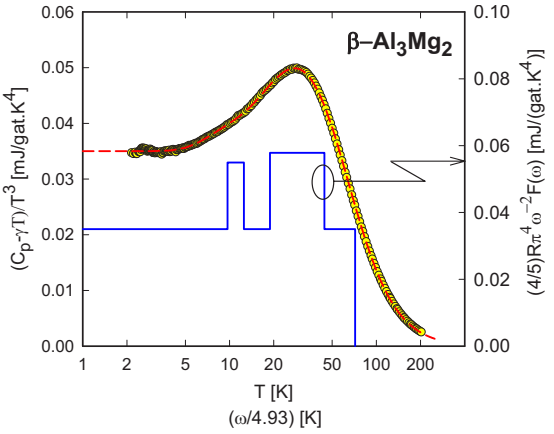

FIG. 3. (Color online) Temperature dependent specific heat C_p of β-Al_3Mg_2, plotted as $(C_p-\gamma T)/T^3$ vs ln T. The dashed line is a least squares fit of the experimental data using the model described in the text with two Einstein modes $\omega_{EL1}=55$ K with width of 14 K and $\omega_{EL2}=150$ K with width of 116 K. The Debye temperature $\theta_D=354$ K. The solid line sketches the phonon spectral function $F(\omega)$ plotted as $(5/4)R\pi^4\omega^{-2}F(\omega)$ vs $\omega/4.93$, where ω is given in kelvin.

$=6.6$ mJ/mol K^2, is subtracted in this plot. Obviously, the heat capacity of β-Al_3Mg_2 deviates from a Debye-like behavior almost in the entire temperature range studied.

The deviations from the simple Debye model imply a rather complicated phonon spectrum present in this compound. In order to qualitatively and quantitatively describe the lattice dynamics, we have adapted a model which incorporates some fine structure in the phonon density of states (see Refs. 18 and 19). The latter is represented by a spectral function $F(\omega)$, allowing to express the heat capacity as

$$C_{ph}(T) = 3R\int_0^\infty F(\omega)\frac{\left(\frac{\omega}{2T}\right)^2}{\sinh^2\left(\frac{\omega}{2T}\right)}d\omega, \qquad (7)$$

with ω the phonon frequency and R the gas constant. The most common assumptions on $F(\omega)$ are $F(\omega)=\delta(\omega)$ and $F(\omega)=\omega^2$ up to a cut-off frequency ω_D, corresponding to the well known Einstein and Debye models, respectively. Junod *et al.*[19] demonstrated that certain functionals of the phonon specific heat take the form of convolutions of the phonon spectrum. Particularly, $(5/4)R\pi^4C_{ph}T^3$ is an image of the spectrum $\omega^{-2}F(\omega)$ for $\omega=4.93T$, where ω is expressed in kelvin. Based on these considerations, we have constructed an elementary phonon spectrum and have carried out least squares fits to the data. In the first approximation, we have assumed that besides a Debye density of states, the system is composed of two additional, energetically separated Einstein-like modes. However, different to standard Einstein models of the specific heat, a certain frequency width for each Einstein branch is allowed. Results of this procedure are shown in Fig. 3. The overall goodness of the fit is extremely high ($r^2=0.999$), revealing a Debye temperature $\theta_D=354$ K, in well agreement with the above indicated low temperature

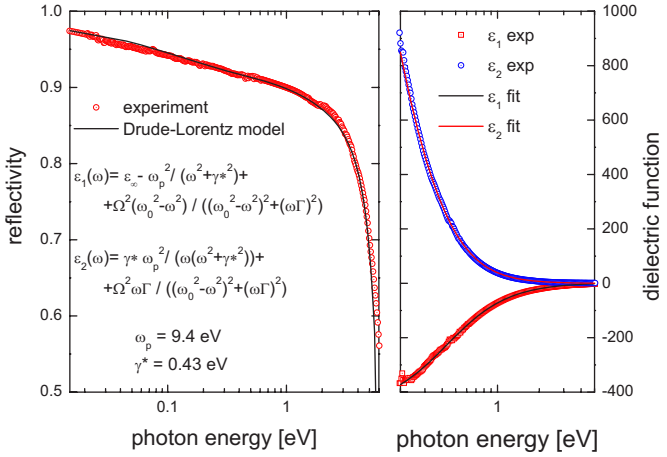

FIG. 4. (Color online) Optical reflectivity and complex dielectric function of β-Al_3Mg_2.

estimation. Two block-shaped Einstein-like contributions are derived, centered at $\omega_{EL1}=55$ K and $\omega_{EL2}=150$ K, with corresponding spectral widths of 14 and 116 K, respectively. Based on this fit, the phonon spectrum is constructed and plotted in Fig. 3, referring to the right axis (solid line). The spectral weight follows from the advisement that for $T=0$, the height of the phonon density of states coincides with the extrapolated value of C_p/T^3 for $T\rightarrow 0$. Both contributions have different spectral weights; the height of these contributions appears to be small sized, implying only to weaker corrections of a Debye spectrum. The substantial width of the upper Einstein-like contribution may represent the complex phonon DOS composed from a superposition of various single Einstein modes, in line with the exceptionally complex crystal structure of β-Al_3Mg_2. Such an extraordinary width of phonon branches was not found in other complicated structured materials such as cage-forming compounds like skutterudites and clathrates.[20]

Optical reflectivity was Kramers-Kronig (KK) transformed to obtain both the real and the imaginary part of the dielectric function, ϵ_1 and ϵ_2, respectively. Ellipsometric data were used to correct the effects of light scattering at the highest energies and to check the results of KK. Results are shown in Fig. 4. The spectrum exhibits a typical metallic behavior, allowing to use the Drude model; appropriate formulas are shown in Fig. 4. One Lorentz oscillator has been added to account for some deficiencies of the model at the largest energies and improve the fit result in this region. This additional oscillator can be ascribed to interband transitions, likely to occur in a complex system such as β-Al_3Mg_2. The spectral weight of this contribution is small ($\Omega=4$ eV, $\Gamma=2.3$ eV, $\omega_0=0.9$ eV) and does not affect the values of the Drude term. The plasma frequency $\hbar\omega_p$ turns out to be 9.4 eV and the scattering term $\hbar\gamma^*=0.43$ eV corresponds to a relatively low scattering time $\tau=1.53\times10^{-15}$ s. Taking into account the Drude model for conductivity results in $\sigma_0=\omega_p^2/(4\pi\gamma^*)=4.48\times10^{16}$ s^{-1}, corresponding to a room temperature resistivity $\rho_{RT}=37$ $\mu\Omega$ cm. The latter is in excellent agreement with the static resistivity data [compare Fig. 1(a)], consolidating the analysis presented.

In order to evaluate the effective mass m of the charge carriers of β-Al_3Mg_2 from the plasma frequency, we have

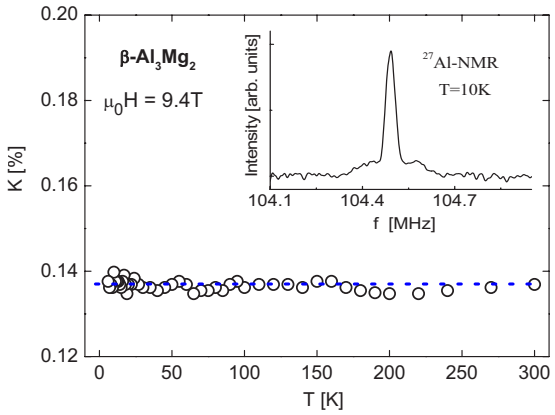

FIG. 5. (Color online) Temperature dependence of the Knight shift (^{27}Al) of β-Al_3Mg_2 at $H=9.4$ T. The inset shows the ^{27}Al spectrum at 10 K.

carried out Hall effect measurements, yielding an almost constant value $n=1.5\times10^{23}$ cm^{-3} for temperatures below 100 K. Using

$$\omega_p^2 = \frac{4\pi ne^2}{m}, \tag{8}$$

with e the electron charge, allows estimation of the effective mass m. With $\hbar\omega_p=9.4$ eV and $m^*=m/m_e$ (m_e is the electron mass), it follows that $n/m^*=0.64\times10^{23}$ cm^{-3}. In the context of the Hall carrier density, the mass enhancement m^* is then of the order of 2. Inspecting data of the pure elements reveals $n_{Al}=1.8\times10^{23}$ cm^{-3} and $n_{Mg}=0.86\times10^{23}$ cm^{-3}; an average would then be $n_{av}=1.5\times10^{23}$ cm^{-3}. This coincidence suggests that the electronic structure of β-Al_3Mg_2 does not differ substantially from a superposition of the electronic structures of the constituent elements. A very recent study of the electronic structure of β-Al_3Mg_2 using soft x-ray spectroscopy, however, evidenced a d-state-like feature near the Fermi energy, absent in pure Al, as well as Mg.[21] This may then explain the effective charge carrier mass $m^*\approx2$.

Some information on the electronic structure of β-Al_3Mg_2 can be gained from NMR studies as well. Data on polycrystalline β-Al_3Mg_2 were recently reported by Dolinsek *et al.*,[7] while the present study is made on single crystalline β-Al_3Mg_2.

A narrow NMR spectrum of the central $\pm1/2\leftrightarrow\mp1/2$ transition for $I=5/2$ nuclear spin of ^{27}Al was observed. The full width at half intensity amounts to 14 kHz at $\mu_0H=9.4$ T, being temperature independent. Besides, a broadened spectrum of the quadrupole split satellite with small intensity around the central line is obvious from the inset of Fig. 5. The spectrum extends over a frequency interval of about 300 kHz, and the nuclear quadrupole frequency $\nu_Q[=3e^2qQ/2I(2I-1)]$ amounts to about 250 kHz. Here, q is the electrical field gradient and Q is the nuclear quadrupole moment. These observations imply the existence of a nonvanishing electric field gradient at the Al site and corroborates the low symmetric environment around Al, as expected from the complex structure of β-Al_3Mg_2.

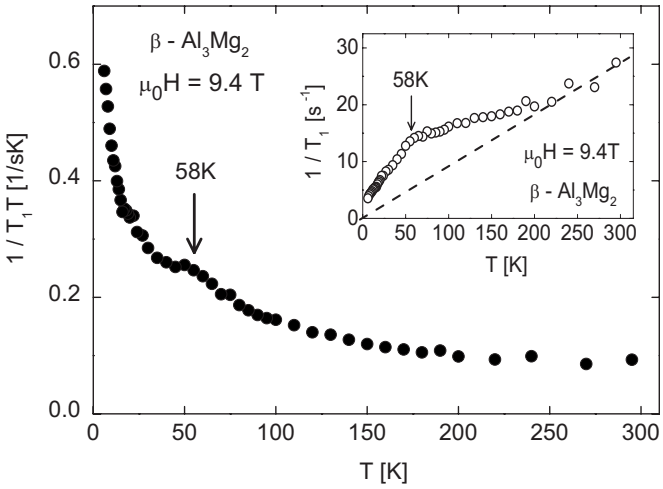

FIG. 6. Temperature dependence of the nuclear spin-lattice relaxation rate of β-Al_3Mg_2. The main panel displays $1/T_1T$ vs T and the inset shows a $1/T_1$ vs T plot. The broken line refers to a T_1T =const relation.

Figure 5 shows the temperature dependent Knight shift determined from the peak position. As the second order quadrupole shift of the central line is negligibly small, the shift derives purely from magnetic origins. The nearly symmetric shape of the spectrum shows that the anisotropy of the Knight shift is very small. The Knight shift is almost temperature independent between 4.3 and 300 K, as shown in Fig. 5, and amounts to +0.135%, which is close to the value of +0.162% in fcc Al metal.[22] The former coincides well with the figures derived previously from polycrystalline materials.[7] The Knight shift is a measure of the local electronic spin density at a specific nuclear site. In general, the Knight shift follows from $K=A_{hf}\chi_{Pauli}$, where A_{hf} is a hyperfine coupling constant, dominated by the Fermi-contact interaction for s electrons at the Fermi level; χ_{Pauli} is the Pauli paramagnetic susceptibility given by $2\mu_BN(E_F)$. Therefore, it follows that the local density of states (LDOS) at the Fermi level of β-Al_3Mg_2 does not substantially differ from that of pure Al.

The measurements of the NMR nuclear spin-lattice relaxation rate T_1 were done by the method of saturation of the central line and a subsequent monitoring of the nuclear magnetization recovery $M(t)$ at variable delay times t. The relaxation rate defined as $1/T_1=2W$, where W represents the spectral density of the fluctuating internal magnetic fields, was extracted by fitting the data to the recovery function, $M(t)/M(\infty)=1-\exp[-(2Wt)^{1/2}]$, which is obtained for the case that T_1 is widely distributed.[23] Least squares fits yield good agreement in the entire temperature range. These results are presented in Fig. 6 as $1/T_1T$ vs T (main panel) and $1/T_1$ vs T (in the inset). Contrary to the relaxation rate expected for a metal, where T_1T remains constant, $1/T_1T$ of β-Al_3Mg_2 increases with decreasing temperature. Additionally, a cusp-type anomaly is observed around 58 K and $1/T_1T$ rapidly rises below that temperature. This suggests contributions from dynamical features of the electron-electron interaction, becoming enhanced at low temperature. A plot of the data according to $1/T_1$ vs T (inset of Fig. 6)

reveals additional intensity below ≈200 K, with a broad peak around 58 K.

The principal relaxation mechanism of the ^{27}Al nucleus is the Fermi-contact interaction, also dominating the Al Knight shift. For a metal with *s* electrons, $1/T_1T$ is directly proportional to the square of LDOS, i.e., $1/T_1T \propto k_B N(E_F)^2$. The value of $1/T_1T=0.1$ (s K)$^{-1}$ obtained at the high temperature limit, apart from the additional contribution below 250 K (shown by the broken line in the inset of Fig. 6), is also comparable with pure Al metal. Thus, NMR results suggest that the DOS of β-Al_3Mg_2 compound is close (at most 50% smaller) to that of Al metal and that electronic correlations are of minor importance.

At present, the origin of the anomalous enhancement of $1/T_1$ with decreasing temperature, which is only observed in $1/T_1$ but not in Knight shift, remains unclear. Its dynamical features, however, remain without relevance for static magnetic qualities.

B. Superconducting and normal state parameters of β-Al_3Mg_2

The above indicated values of the thermodynamic and the upper critical field, $H_c(0) \simeq 7.6$ mT and $H_{c2}(0) \simeq 0.14$ T, are used to calculate the ratio of the spatial variation length of the local magnetic field $\lambda_{GL}(0)$ to the coherence length $\xi_{GL}(0)$ via Abrikosov's relation $\lambda_{GL}(0)/\xi_{GL}(0) \equiv \kappa_{GL}(0) = H_{c2}/[\sqrt{2}H_c(0)]$ yielding the Ginzburg-Landau parameter $\kappa_{GL}=13(2)$ for β-Al_3Mg_2.

The absolute values of the coherence length ξ_0 and the penetration depth $\lambda(0)$ can be evaluated with the basic equations of the isotropic Ginzburg-Landau-Abrikosov-Gor'kov theory:

$$\kappa(T) = \frac{2\pi\sqrt{2}\mu_0 H_c(T)\lambda_{GL}^2(T)}{\Phi_0} \tag{9}$$

and

$$\mu_0 H_{c2}(T) = \frac{\Phi_0}{2\pi\xi_{GL}^2(T)}, \tag{10}$$

with $\Phi_0=h/2e$, the fluxoid quantum. The values obtained thereby are $\lambda_{GL}(0)=\kappa\sqrt{\frac{\Phi_0}{2\pi\mu_0 H_{c2}}}=5.3\times10^{-7}$ m and $\xi_{GL}(0) \simeq 4.85\times10^{-8}$ m. The very large value of $\kappa \simeq 13$ as compared to $\kappa \sim 0.03$ for pure Al (Ref. 26) is, at least partially, a consequence of the largely reduced mean free path, as inferred from the large residual resistivity $\rho_0=33.3$ $\mu\Omega$ cm of β-Al_3Mg_2. Using the Gor'kov-Goodman relation,[27] $\kappa=\kappa_0 + 0.0237\sqrt{\gamma\rho_0}$, where κ_0 is the clean limit value of the Ginzburg-Landau parameter, γ is the Sommerfeld coefficient in units of J/m^3 K^2, and ρ_0 is the residual resistivity in $\mu\Omega$ cm, yields $\kappa \simeq 8.3$ if $\kappa_0 \sim \kappa_{Al}$. The experimental value $\kappa \simeq 13$ provides a rough estimate of $\kappa_0 \sim 5$ for β-Al_3Mg_2 in the hypothetical clean limit case.

In the following, we estimate a set of typical parameters from an analysis of superconducting and normal state properties in terms of the BCS theory,[24] assuming a spherical Fermi surface. Starting parameters are $\gamma_s=0.0066$ J/mol K^2, $\mu_0 H'_{c2}=-0.2$ T/K, $\mu_0 H_{c2}(0) \approx 0.14$ T, and $\rho_0=33.3$ $\mu\Omega$ cm. The transition temperature into the superconducting ground state as observed from heat capacity data is 0.87 K.

The effective Fermi surface S_s^{dl} is computed[24,25] as $S_s^{dl} \simeq 2.1\times10^{20}$ m^{-2} for the dirty limit. Within this limit, $\mu_0 H'_{c2}(\text{calc})=4490\gamma\rho_0=-0.16$ T/K, well in agreement with the experimental data [compare Fig. 1(b)]. Combining the Fermi surface with γ_s gives the Fermi velocity $v_F \simeq 36\,600$ m/s and in the context of the residual resistivity $\rho_0=33.3$ $\mu\Omega$ cm, a mean free path $l_{tr} \simeq 5.5\times10^{-8}$ m can be derived. The coherence length ξ_0 for $T\to0$ follows from the BCS equation, $\xi_0=0.18\hbar v_F/(k_B T_c) \simeq 5.6\times10^{-8}$ m. κ can be derived from $\kappa=529H'_{c2}/\gamma_s^{1/2} \approx 10.2$, while the London penetration depth follows from $\lambda_L(0) \approx 5.04\times10^{12}\gamma_s^{1/2}/S_s=6.3\times10^{-7}$ m. In spite of the very complex crystalline structure of β-Al_3Mg_2, the system does not behave like typical amorphous superconductors[28,29] since both the coherence length and the mean free path are almost one order of magnitude larger than the largest unit cell dimension of β-Al_3Mg_2. Additionally, amorphous superconductors are characterized by an extended linearity of $H_{c2}(T)$, while $H_{c2}(T)$ of β-Al_3Mg_2, within the experimental resolution, is rather curvilinear.

The parameters κ, ξ_0, and $\lambda_L(0)$, evaluated from the upper and the thermodynamic critical field, excellently agree with model calculations based on the free electron model. This allows to conclude that, although the crystal structure of β-Al_3Mg_2 is rather complicated, the relevant parts of the electronic structure remain rather isotropic. The fact that $l_{tr}/\xi \approx 1$ classifies β-Al_3Mg_2 as a dirty limit superconductor, while $\kappa \approx 13$ indicates type II superconducting behavior.

IV. SUMMARY

Based on low temperature electrical resistivity and specific heat measurements, we have shown that β-Al_3Mg_2 undergoes a phase transition into a superconducting ground state at $T_c=0.87$ K. Microscopically, superconductivity can be understood in terms of the phonon-mediated BCS model. An exponential behavior of the specific heat well below T_c implies a nodeless superconducting gap in the electronic density of states, of the order of $\Delta \approx 1.6$ K. The initial slope of the upper critical field is deduced as $\mu_0 H'_{c2} \approx -0.2$ T/K, while an extrapolation $T\to0$ yields $\mu_0 H_{c2}(0) \approx 0.14$ T. The limiting pair breaking mechanism seems to be orbital pair breaking, as concluded from the model of Werthamer *et al.*[12]

Superconductivity in β-Al_3Mg_2 occurs in a crystal environment without inversion symmetry. Broken inversion symmetry has a distinct influence on the superconducting phase, which usually relies on the formation of pairs of electrons in degenerate states with opposite momentum. The availability of such states is normally guaranteed by time reversal and inversion symmetries.[30,31] The absence of inversion symmetry would favor a strong antisymmetric spin-orbit coupling and, as a consequence, a mixture of spin-singlet and spin-triplet pairs in the superconducting condensate can be expected.[32] The small values of the upper critical field, however, seem to exclude a substantial portion of spin-triplet pairs in the condensate. Moreover, the lightweight elements Al and Mg may be responsible for only a minimal spin-orbit coupling in β-Al_3Mg_2; hence, the spin-singlet condensate

dominates. Additionally, the very complex crystal structure is supposed to smooth the effect of the missing inversion symmetry. A rather conventional superconductivity seems to appear, which also follows from the agreement of the upper critical field with Werthamer's model. Presently, only a small number of superconductors without inversion symmetry have been found. For a recent review on this subject, see, e.g., Ref. 33.

Although the crystal structure of β-Al_3Mg_2 appears to be rather complicated, the various physical quantities derived in both the superconducting and the normal state region turn out to be simple. In the first approximation, some of these quantities even look like a balanced superposition of pure Al and Mg. The latter follows from macroscopic measurements such as the specific heat and microscopic data like those derived from NMR as well.

ACKNOWLEDGMENTS

This work was supported by the European Network of Excellence on Complex Metallic Alloys supported by EU under Contract No. NMP3-CT-2005-500140, by the Austrian Science Foundation, Project No. FWF-P-18054, and by the Romanian Project Ceex M3-204/2006.

[1] L. Pauling, J. Am. Chem. Soc. **45**, 2777 (1923).
[2] G. Bergman, J. L. T. Waugh, and L. Pauling, Acta Crystallogr. **10**, 254 (1957).
[3] M. Boudard, H. Klein, M. de Boissieu, M. Audier, and H. Vincent, Philos. Mag. A **74**, 939 (1996).
[4] K. Urban and M. Feuerbacher, J. Non-Cryst. Solids **334-335**, 143 (2004).
[5] S. Samson, Acta Crystallogr. **19**, 401 (1965).
[6] M. Feuerbacher *et al.*, Z. Kristallogr. **222**, 259 (2007).
[7] J. Dolinsek *et al.*, Intermetallics **15**, 1367 (2007).
[8] M. Lipinska-Chwalek, S. Balanetskyy, C. Thomas, S. Roitsch, and M. Feuerbacher, Intermetallics (to be published).
[9] R. Bachmann *et al.*, Rev. Sci. Instrum. **43**, 205 (1972).
[10] D. W. Woodward and G. D. Cody, Phys. Rev. **136**, A166 (1964).
[11] R. Caton and R. Viswanathan, Phys. Rev. B **25**, 179 (1982).
[12] N. R. Werthamer, E. Hefland, and P. C. Hohenberg, Phys. Rev. **147**, 295 (1966).
[13] K. M. Wong, E. J. Cotts, and S. J. Poon, Phys. Rev. B **30**, 1253 (1984).
[14] K. Maki, Phys. Rev. **148**, 362 (1966).
[15] C. Wälti, E. Felder, M. A. Chernikov, H. R. Ott, M. de Boissieu, and C. Janot, Phys. Rev. B **57**, 10504 (1998).
[16] W. L. McMillan, Phys. Rev. **167**, 331 (1968).
[17] B. Mühlschlegel, Z. Phys. **155**, 313 (1959).
[18] A. Junod, D. Bichsel, and J. Muller, Helv. Phys. Acta **52**, 580 (1979).
[19] A. Junod, T. Jarlborg, and J. Muller, Phys. Rev. B **27**, 1568 (1983).
[20] St. Berger, Ph.D. thesis, TU Wien, 2003.
[21] E. Belin and J. M. Dubois (unpublished).
[22] G. C. Cater, L. H. Bennet, and D. J. Kahan, Progress in Material Science (Pergamon, New York, 1977).
[23] K. Kumagai and F. Y. Fradin, Phys. Rev. B **27**, 2770 (1983).
[24] See, for example, M. Tinkham, *Introduction to Superconductivity* (McGraw-Hill, New York, 1975).
[25] See, for example, R. R. Hake, Phys. Rev. **158**, 356 (1967).
[26] See, for example, C. P. Poole, H. A. Farach, and R. J. Creswick, *Superconductivity* (Academic, San Diego, 1995).
[27] L. P. Gorkov, Zh. Eksp. Teor. Fiz. **37**, 1407 (1959) [Sov. Phys. JETP **10**, 998 (1960)]; B. B. Goodman, IBM J. Res. Dev. **6**, 62 (1962).
[28] W. L. Johnson, S. J. Poon, and P. Duwez, Phys. Rev. B **11**, 150 (1975).
[29] W. L. Johnson and S. J. Poon, J. Appl. Phys. **46**, 1787 (1975).
[30] P. W. Anderson, J. Phys. Chem. Solids **11**, 26 (1958).
[31] P. W. Anderson, Phys. Rev. B **30**, 4000 (1984).
[32] L. P. Gor'kov and E. I. Rashba, Phys. Rev. Lett. **87**, 037004 (2001).
[33] E. Bauer, H. Kaldarar, A. Prokofiev, E. Royanian, A. Amato, J. Sereni, W. Brämer-Escamilla, and I. Bonalde, J. Phys. Soc. Jpn. **76**, 051009 (2007).